Journal of Japan Association for Earthquake Engineering, Vol. 20, No. 5, 2020

DEVELOPMENT OF INFERENCE METHODS FOR ROTATIONAL MOTIONS ON GROUND SURFACE AND APPLICATION TO MICROTREMORS ACQUIRED WITH A SMALL-SIZE DENSE ARRAY

Koji HADA[1] and Masanori HORIKE[2]

[1] Architectural Group, NEWJEC Inc., Osaka, Japan, hadakj@newjec.co.jp
[2] Member, Advisor, Division of Engineering, Hanshin Consultants Co., Ltd, Osaka, Japan, horike@hanshin-consul.co.jp

ABSTRACT: In this study, we develop two methods for the inference of rotation vector on ground surface, two rocking rotations and a single torsional rotation. The first, termed nth-order elastic method, is based on the elasticity of the ground surface. The rotation vector is constructed from the first derivative with respect to the space of the ground surface motions. The first derivative is calculated from simultaneous equations by n-th order Taylor expansion obtained by difference motion between multiple observation points. Meanwhile, the second, termed rigid method, is based on the rigidity of ground surface and the rotation.

Keywords: Inference methods of rotational motions, Ground surface, Microtremors, Small-size dense array

1. INTRODUCTION

Over the years, many reports and studies have noted the possibility that buildings were damaged by torsional vibration[1)-3)], including many reports concerning the 1995 Hyogoken-Nanbu Earthquake[4)]. Damage due to torsional vibration was also reported for the 2016 Kumamoto Earthquakes in April 2016[5)]. In these reports and studies, the causes of the torsional vibration have generally been sought in the eccentricity of the buildings, and virtually no consideration has been given to the influence of rotational inputs. For the earthquake-resistant design, there are regulations covering the translational components of seismic inputs, but the rotational inputs are not regulated. As a result, the rotation components of seismic inputs are not taken into account. Nevertheless, it is thought that there is insufficient observational evidence to confirm that they do not need to be taken into account[6)]. For instance, a report by Hada and Horike[7)] suggests that, for microtremors at least, the rotational inputs to the foundations of a building are too large to be disregarded. Two likely reasons why rotational inputs have not been taken into account to date are that it is not easy to conduct dense array seismic observations covering a scale such as that of the foundations of a building, and that techniques for assessing the rotation components recorded by the array have not been sufficiently established.

As described later, rotation components are bound to exist on the ground surface whenever seismic motions exhibit spatial variation. In other words, with the exception of vertically-incident plane P- and S-waves, rotation components necessarily exist. And as vertically-incident plane waves are a practical

impossibility in actual seismic motions, there are always rotational inputs. Consequently, the issue is not whether seismic motions include rotation components, but the scale of the rotation components.
As far as the authors are aware, the only study in Japan that assumes the influence of rotational inputs on building vibration was conducted by Yagi *et al*[8]. Outside Japan, there have been studies concerning the assessment of rotation components of seismic data acquired using the Chiba Array and dense arrays at Rotung, Taiwan[9)-11)]. Discussion of the relationship between maximum velocity and maximum angular acceleration has also commenced[11)]. However, studies concerning the assessment of rotational inputs cannot be said to be sufficient in either quantitative or qualitative terms. Consequently, making use of small-size dense array seismic observations to increase knowledge concerning rotational inputs is a significant topic for study. As a result of progress in the development of seismic instruments, observations using small-size (of a scale similar to the foundations of a building) dense arrays such as the Chiba array[12)] are becoming less difficult, and many such observations may be conducted in the near future.

Given these circumstances, this report begins by proposing a number of methods for inference of the three rotation components from seismic data acquired using a dense plane array deployed on a free surface, and describing the relationships between them. Next, microtremor observation with small-size dense microtremor array conducted in order to apply each of these inference methods. Finally, it describes the findings acquired by applying the rotation component inference methods to microtremor array data. Specifically, it describes findings concerning appropriate array configurations for obtaining the rotation components, and the inference and results for size of rotation components and for a region behaving as a rigid body with respect to rotation of rotation components. As described in Section 2 below, in mathematical terms, the zone behaving as a rigid body with respect to rotation is the zone infinitesimally close to the reference site. However, it is considered that a limited zone may exist wherein the size of the rotation components centered on the reference site hardly varies. Such a zone that behaves as a rigid body with respect to rotation is important in engineering terms.

2. ESTIMATION METHOD OF ROTATION COMPONENTS USING SMALL-SIZE DENSE ARRAY DATA

2.1 Elastic body

Consider a semi-infinite elastic body with coordinate axes as shown in Fig. 1. The displacements from a reference site $\boldsymbol{X} = \{x_1 \ x_2 \ x_3\}^T$ within the elastic body to two points separated by a sufficiently small distance $\boldsymbol{\delta X} = \{\delta x_1 \ \delta x_2 \ \delta x_3\}^T$ are expressed in Lagrangian representation as $\boldsymbol{u}(\boldsymbol{X})$ and $\boldsymbol{u}(\boldsymbol{X} + \boldsymbol{\delta X})$. Here, bold face signifies a vector, and the expressions in the braces are the components of the vector. The relative displacement with respect to the reference site $\boldsymbol{\delta u} = \boldsymbol{u}(\boldsymbol{X} + \boldsymbol{\delta X}) - \boldsymbol{u}(\boldsymbol{X})$,

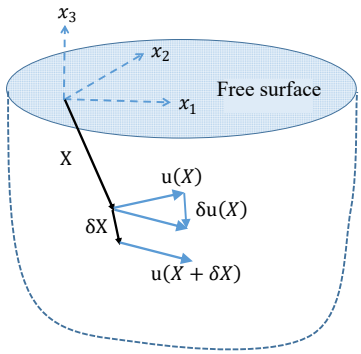

Fig. 1 Coordinate system and definition of relative displacement δu

can be expressed as

$$\boldsymbol{\delta u} = \begin{Bmatrix} \delta u_1 \\ \delta u_2 \\ \delta u_3 \end{Bmatrix} = \begin{bmatrix} \varepsilon_{11} & \varepsilon_{12} & \varepsilon_{13} \\ \varepsilon_{21} & \varepsilon_{22} & \varepsilon_{23} \\ \varepsilon_{31} & \varepsilon_{32} & \varepsilon_{33} \end{bmatrix} \begin{Bmatrix} \delta x_1 \\ \delta x_2 \\ \delta x_3 \end{Bmatrix} + \begin{Bmatrix} \omega_1 \\ \omega_2 \\ \omega_3 \end{Bmatrix} \times \begin{Bmatrix} \delta x_1 \\ \delta x_2 \\ \delta x_3 \end{Bmatrix} \tag{1}$$

as well known form, for example, Aki and Richards[13]. The first term on the right of the equation indicates the contribution of deformation such as shear deformation or expansion-contraction deformation to the relative displacement. In the second term, $\omega_i, (i = 1,2,3)$ expresses the rigid body rotation angle about the x_i axis if the condition $\|\omega_i\| \ll 1$ is met, and the second term indicates the relative displacement due to rigid body rotation. The relationship between the infinitesimal rotation angle $\{\omega_1 \ \omega_2 \ \omega_3\}^T$ and displacement is expressed as

$$\begin{Bmatrix} \omega_1 \\ \omega_2 \\ \omega_3 \end{Bmatrix} = \frac{1}{2} \boldsymbol{\nabla} \times \boldsymbol{u}(\boldsymbol{X}) = \frac{1}{2} \begin{Bmatrix} \dfrac{\partial u_3}{\partial x_2} - \dfrac{\partial u_2}{\partial x_3} \\ \dfrac{\partial u_1}{\partial x_3} - \dfrac{\partial u_3}{\partial x_1} \\ \dfrac{\partial u_2}{\partial x_1} - \dfrac{\partial u_1}{\partial x_2} \end{Bmatrix} \tag{2}$$

The $\boldsymbol{\nabla}$ symbol signifies the three-dimensional nabla operator. From Eq. (2), it can be seen that if the seismic motion includes spatial variation, rotation components will necessarily be generated, and that their values can be calculated from the six partial derivatives relating to the spatial coordinates of the seismic motion displacement. It also makes it possible to anticipate that rotation components will be large in situations such as cases where strong scattered waves occur and cases where there are prominent surface waves with short wavelengths.

When attempting to use Eq. (2) to calculate the rotation angles, an awkward issue arises. To calculate the rotation angles ω_1 and ω_2, the partial derivatives $\frac{\partial u_2}{\partial x_3}$ and $\frac{\partial u_1}{\partial x_3}$ are required. And because these two partial derivatives are values relating to the x_3 axis (depth axis), data of observations made underground are required. In other words, to calculate the rotation components using Eq. (2), a 3-dimensional array including seismometers underground is required instead of a 2-dimensional array with seismometers only on the ground surface. However, acquiring seismic data with a 3-dimensional array that requires seismic observations to be made inside boreholes is not a simple matter. To resolve that issue, the free surface condition is used to replace the two partial derivatives relating to the depth direction with partial derivatives relating to the horizontal plane.

In a free surface the x_1 direction and x_2 direction components of traction, τ_{13} and τ_{23}, are both zero. This condition can be expressed as

$$\begin{Bmatrix} \tau_{13} \\ \tau_{23} \end{Bmatrix} = 2G \begin{Bmatrix} \varepsilon_{13} \\ \varepsilon_{23} \end{Bmatrix} = G \begin{Bmatrix} \dfrac{\partial u_1}{\partial x_3} + \dfrac{\partial u_3}{\partial x_1} \\ \dfrac{\partial u_3}{\partial x_2} + \dfrac{\partial u_2}{\partial x_3} \end{Bmatrix} = \begin{Bmatrix} 0 \\ 0 \end{Bmatrix} \tag{3}$$

where G is the shear modulus. Using Eq. (3), Eq. (2) can be rewritten as follows.

$$\begin{Bmatrix}\omega_1\\ \omega_2\\ \omega_3\end{Bmatrix}=\begin{Bmatrix}\dfrac{\partial u_3}{\partial x_2}\\ -\dfrac{\partial u_3}{\partial x_1}\\ \dfrac{1}{2}\left(\dfrac{\partial u_2}{\partial x_1}-\dfrac{\partial u_1}{\partial x_2}\right)\end{Bmatrix} \tag{4}$$

From this expression, it can be seen that it is possible to calculate the rotation components from the four partial derivatives inferred from the data acquired by a 2-dimensional array on the ground surface. Hereinafter, this report concerns inference methods using the 2-dimensional array data for these four partial derivatives.

When the reference observation site coordinates are taken to be $(x_{10},\ x_{20})$ and the coordinates of the nearby observation site j are taken to be $(x_{10}+\delta x_{1j},\ x_{20}+\delta x_{2j})$, δu_{ij}, the i component of relative displacement (or differential motion) for observation site j relative to the reference site, can be expressed, using Taylor series expansion and binomial theorem, as

$$\delta u_{ij}=u_i\left(x_{10}+\delta x_{1j},x_{20}+\delta x_{2j}\right)-u_i(x_{10},x_{20})\cong\sum_{k=1}^{n}\frac{1}{k!}\left(\delta x_{1j}\frac{\partial}{\partial x_1}+\delta x_{2j}\frac{\partial}{\partial x_2}\right)^k u_i$$

$$=\sum_{k=1}^{n}\sum_{l=0}^{k}\frac{\left(\delta x_{1j}\right)^{k-l}}{(k-l)!}\frac{\left(\delta x_{2j}\right)^{l}}{l!}\frac{\partial^k u_i}{\partial x_{1j}^{k-l}\partial x_{2j}^{l}}\qquad(j=1,2,\cdots,n) \tag{5}$$

Substituting the observed differential motion into the left side of the expression creates an equation system with the partial differential on the right side as an unknown. Resolving this gives the first-order partial derivatives, which can be substituted into Eq. (4) to obtain the rotation components.

Cases using first- and second-order Taylor expansion (n = 1,2) are shown here as examples of this approach. With a first-order expansion, the unknowns are the two partial derivatives $\frac{\partial u_i}{\partial x_1}$ and $\frac{\partial u_i}{\partial x_2}$. Consequently, the expression can be solved if there are 2 observation sites in addition to the reference site (3 observation sites in total). If the number of observation sites excluding the reference sites is $m \geq 2$, the equation system to be solved is

$$\begin{Bmatrix}\delta u_{i1}\\ \delta u_{i2}\\ \vdots\\ \delta u_{im}\end{Bmatrix}=\begin{bmatrix}dx_{11} & dx_{21}\\ dx_{12} & dx_{22}\\ & \vdots\\ dx_{1m} & dx_{2m}\end{bmatrix}\begin{Bmatrix}\dfrac{\partial u_i}{\partial x_1}\\ \dfrac{\partial u_i}{\partial x_2}\end{Bmatrix}\qquad(i=1,2,3) \tag{6}$$

When a second-order Taylor expansion is applied, by using a number of observation sites excluding the reference site $m\geqq5$, the equation system to be solved is

$$\begin{Bmatrix} \delta u_{i1} \\ \delta u_{i2} \\ \vdots \\ \delta u_{im} \end{Bmatrix} = \begin{bmatrix} dx_{11} & dx_{21} & 0.5(dx_{11})^2 & dx_{11}dx_{21} & 0.5(dx_{21})^2 \\ dx_{12} & dx_{22} & 0.5(dx_{12})^2 & dx_{12}dx_{22} & 0.5(dx_{22})^2 \\ & & \vdots & & \\ dx_{1m} & dx_{2m} & 0.5(dx_{1m})^2 & dx_{1m}dx_{2m} & 0.5(dx_{2m})^2 \end{bmatrix} \begin{Bmatrix} \frac{\partial u_i}{\partial x_1} \\ \frac{\partial u_i}{\partial x_2} \\ \frac{\partial u_i^2}{\partial x_1^2} \\ \frac{\partial u_i^2}{\partial x_1 \partial x_2} \\ \frac{\partial u_i^2}{\partial x_2^2} \end{Bmatrix} \quad (i = 1,2,3) \tag{7}$$

where $dx_{1j} = (x_{1j} - x_{10})$, $dx_{2j} = (x_{2j} - x_{20})$. Also, j=1,2,... , m. Similarly, when using an nth-order Taylor expansion, the number of unknown partial differentials is $\frac{n(n+3)}{2}$. The number of observation sites, including the reference observation site, must be at least as large as the number of unknown partial differentials. Expressions (5), (6), (7) are the same as those given in Basu *et al*[10]. for acceleration gradient method of order n (AGMn). Equation systems generated as described above can be solved using the weighted least squares method[14] to obtain the rotation angles. The weighting matrix is the same as described by Spudich *et al*[15]. The method of inference of rotation angles assuming an elastic body and using an nth-order Taylor series expansion is hereinafter called the nth-order elastic method.

2.2 Rigid body

Using a first-order Taylor expansion to approximate differential motion means that differential motion is treated as movement on a plane passing through the reference site for an arbitrary period of time (at a certain moment). In slightly more concrete terms, Eq. (6) is an approximation of differential motion on a plane passing through the origin at gradient $\frac{\partial u_i}{\partial x_1}$ in the δx_1 direction and gradient $\frac{\partial u_i}{\partial x_2}$ in the δx_2 direction. In other words, with the 1st-order elastic method, the zone within which the observation sites are situated is considered to be a rigid body. Consequently, it should be possible to infer the same rotation components as for the 1st-order elastic method by assuming that the ground surface is a rigid body. The following description of rotation component inference methods assumes that the ground surface behaves as a rigid body.

When a rigid body is assumed, the velocity at observation site j $\{\dot{u}_{1j} \;\; \dot{u}_{2j} \;\; \dot{u}_{3j}\}^T$, separated from the reference site by distance $\boldsymbol{\delta X} = \{\delta x_{1j} \;\; \delta x_{2j} \;\; 0\}^T$, is expressed[16], using the translational velocity $\{\dot{u}_{10} \;\; \dot{u}_{20} \;\; \dot{u}_{30}\}^T$ and angular velocity vector $\{\dot{\omega}_1 \;\; \dot{\omega}_2 \;\; \dot{\omega}_3\}^T$ at the reference site, as

$$\begin{Bmatrix} \dot{u}_{1j} \\ \dot{u}_{2j} \\ \dot{u}_{3j} \end{Bmatrix} = \begin{Bmatrix} \dot{u}_{10} \\ \dot{u}_{20} \\ \dot{u}_{30} \end{Bmatrix} + \begin{Bmatrix} \dot{\omega}_1 \\ \dot{\omega}_2 \\ \dot{\omega}_3 \end{Bmatrix} \times \begin{Bmatrix} \delta x_{1j} \\ \delta x_{2j} \\ 0 \end{Bmatrix} \tag{8}$$

Consequently, the differential velocity vector for the reference site is

$$\begin{Bmatrix} \delta\dot{u}_{1j} \\ \delta\dot{u}_{2j} \\ \delta\dot{u}_{3j} \end{Bmatrix} = \begin{Bmatrix} \dot{u}_{1j} \\ \dot{u}_{2j} \\ \dot{u}_{3j} \end{Bmatrix} - \begin{Bmatrix} \dot{u}_{10} \\ \dot{u}_{20} \\ \dot{u}_{30} \end{Bmatrix} = \begin{Bmatrix} \dot{\omega}_1 \\ \dot{\omega}_2 \\ \dot{\omega}_3 \end{Bmatrix} \times \begin{Bmatrix} \delta x_{1j} \\ \delta x_{2j} \\ 0 \end{Bmatrix} = \begin{Bmatrix} -\dot{\omega}_3 \delta x_{2j} \\ \dot{\omega}_3 \delta x_{1j} \\ \dot{\omega}_1 \delta x_{2j} \;\; -\dot{\omega}_2 \delta x_{1j} \end{Bmatrix} \tag{9}$$

Rotation angle velocity is obtained by finding the condition that minimizes the difference between the observed differential velocity and the differential velocity calculated from Eq. (9). Consequently, when a rigid body is assumed, it is possible to obtain the rotation components directly without the need for first-order spatial derivatives of acceleration as were required when an elastic body is assumed.

First of all, using the expressions in the first and second steps of Eq. (9), angular velocity $\dot{\omega}_3$ is

obtained using the least-squares method. The residual sum of squares $f(\dot{\omega}_3)$ for the observed values and predicted values of differential velocity $\delta\dot{u}_1$ and $\delta\dot{u}_2$ is expressed as

$$f(\dot{\omega}_3) = \sum_{j=1}^{m} \left\{ \left(\delta\dot{u}_{1j} + \dot{\omega}_3 \delta x_{2j} \right)^2 + \left(\delta\dot{u}_{2j} - \dot{\omega}_3 \delta x_{1j} \right)^2 \right\} \tag{10}$$

The condition under which this expression minimized is $\frac{\partial f(\dot{\omega}_3)}{\partial \dot{\omega}_3} = 0$. Consequently,

$$\dot{\omega}_3 = \frac{\sum_{j=1}^{m} \left(\delta x_{1j}\ \delta\dot{u}_{2j} - \delta x_{2j}\ \delta\dot{u}_{1j} \right)}{\sum_{j=1}^{m} \left(\delta x_{1j}{}^2 + \delta x_{2j}{}^2 \right)} \tag{11}$$

obtaining the angular velocity for the x_3 axis.

Consider the situation where there is only one observation site apart from the reference site (m = 1). In this situation, Eq. (11) becomes

$$\dot{\omega}_3 = \frac{\delta x_{11}\ \delta\dot{u}_{21} - \delta x_{21}\ \delta\dot{u}_{11}}{\delta x_{11}{}^2 + \delta x_{21}{}^2} = \frac{1}{r} \left(\delta\dot{u}_{21} \cos\theta - \delta\dot{u}_{11} \sin\theta \right) \tag{12}$$

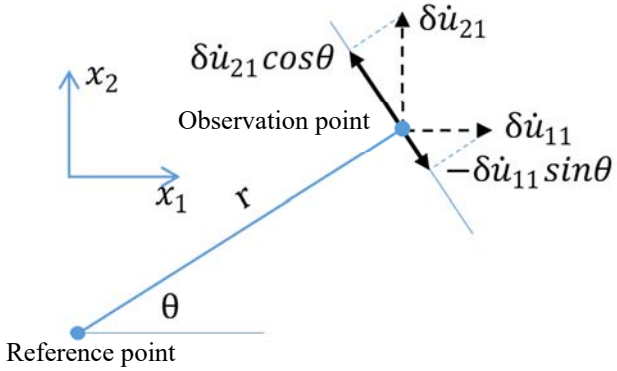

Fig. 2 Explanation for inference of torsion (ω_3) components by the single-site rigid method

In this expression, variables r and θ, as shown in Fig. 2, express the distance between the reference site and observation site, and the angle between a straight line joining the reference site and observation site and the x_1 axis. The significance of this expression is clear. As shown in the figure, projecting the differential velocity for the two horizontal directions at the observation site onto a straight line that is perpendicular to the straight line joining the reference site and observation site, and dividing the sum of the two by distance r, it is possible to obtain the rotation angle velocity $\dot{\omega}_3$.

Next, angular velocities $\dot{\omega}_1$ and $\dot{\omega}_2$ are obtained using the third step of Eq. (9). In this case, the residual sum of squares $g(\dot{\omega}_1, \dot{\omega}_2)$ is

$$g(\dot{\omega}_1\ , \dot{\omega}_2) = \sum_{j=1}^{m} \left(\delta\dot{u}_{3j} - \dot{\omega}_1 \delta x_{2j}\ + \dot{\omega}_2 \delta x_{1j} \right)^2 \tag{13}$$

The conditions for minimizing Eq. (13) are as follows: $\frac{\partial g(\dot{\omega}_1\ ,\dot{\omega}_2)}{\partial \dot{\omega}_1} = \frac{\partial g(\dot{\omega}_1\ ,\dot{\omega}_2)}{\partial \dot{\omega}_2} = 0$.

$$\begin{Bmatrix} \sum_{j=1}^{m} \delta\dot{u}_{3j}\delta x_{1j} \\ \sum_{j=1}^{m} \delta\dot{u}_{3j}\delta x_{2j} \end{Bmatrix} = \begin{bmatrix} \sum_{j=1}^{m} \delta x_{1j}\ \delta x_{2j} & -\sum_{j=1}^{m} \delta x_{1j}{}^{2} \\ \sum_{j=1}^{m} \delta x_{2j}{}^{2} & -\sum_{j=1}^{m} \delta x_{1j}\ \delta x_{2j} \end{bmatrix} \begin{Bmatrix} \dot{\omega}_1 \\ \dot{\omega}_2 \end{Bmatrix} \tag{14}$$

Solving this expression gives the angular velocities $\dot{\omega}_1$ and $\dot{\omega}_2$.

Here also, consider the situation where there is only the reference site and one observation site. In this case, Eq. (14) can not be used because the right-hand side matrix is irregular. It is necessary to return to Eq. (13). If the observation site is assumed to be on the x_1 axis, Eq. (13) becomes $g(\dot{\omega}_1, \dot{\omega}_2) = (\delta\dot{u}_{31} + \dot{\omega}_2\delta x_{11})^2$. The condition under which this expression is minimized is $\dot{\omega}_2 = -\frac{\delta\dot{u}_{31}}{\delta x_{11}}$. From this expression, it can be seen that it is possible to obtain the angular velocity with respect to the x_2 axis by dividing the vertical differential velocity by the distance between the observation site and reference site. Similarly, the angular velocity with respect to the $x_1\ axis$ is $\dot{\omega}_1 = \frac{\delta\dot{u}_{31}}{\delta x_{21}}$. The coordinate axes x_1 and x_2 are used here for convenience. Consequently, the angular velocity $\dot{\omega}_r$ obtained by dividing the vertical differential velocity by the distance between the observation site and the reference site is a good approximation for $\dot{\omega}_1$, $\dot{\omega}_2$. Hereinafter, cases where either Eq. (11) or Eq. (14) is used are referred to as the multi-site rigid method, and cases where Eq. (12) is used are referred to as the single-site rigid method.

Summarizing the above results, angular acceleration obtained by the 1st-order elastic method on the assumption of an elastic body (or in other words, angular acceleration obtained by means of Eq. (6)) is identical to angular acceleration obtained by the multi-site rigid method. Moreover, rotation components $\dot{\omega}_3$ and $\dot{\omega}_r$ can be easily obtained by the single-site rigid method with just one more observation site in addition to the reference site. The relationship between the rotation angle obtained as an elastic body and the rotation angle obtained as a rigid body is discussed in detail in Section 4.

The descriptions in Section 2.1 of the nth-order elastic method assuming an elastic body incorporate displacement and rotation angle, but these can be replaced by acceleration and angular acceleration without any need for further change. As observations are conducted by observing acceleration, the rotation components obtained by the nth-order elastic method are all shown in terms of angular acceleration below. Also, this section described the inference methods for angular velocity as a rigid body. In this case, acceleration data is converted to velocity data by numerical integration, and the method described in this section is used to infer angular velocity before converting to angular acceleration by numerical differentiation. For this reason, hereinafter, the dot above the ω symbol that represents angular acceleration is omitted for convenience. Also, ω_1, ω_2, ω_r will be described as rocking components, and ω_3 as a torsional component.

3. MICROTREMORS ACQUIRED WITH A SMALL-SIZE DENSE ARRAY AND DIFFERENTIAL MOTION CHARACTERISTICS

3.1 Microtremors acquired with a small-size dense array

Small-size dense array seismic observations extend over long periods (several months to several years), which raises issues such as the selection of the array installation site and maintenance of seismic instruments, making it difficult to establish such arrays. To circumvent these issues, this study made observations of microtremors using a small-size dense array that are relatively easy to conduct. The rotation component inference methods described in the preceding section were then applied to the microtremor data acquired. The observations were made at a public park in Osaka City.

According to KuniJiban[17], the borehole data access site operated by Japan's Ministry of Land, Infrastructure, Transport and Tourism, boring data has been published for a number of sites within the park where the observations for this study were made. The boring data shows that to a depth of about

20-30 m, there was silt or sand with an N value of 10 or less, so the ground is envisaged as relatively soft. Below that layer is a foundation with an N value of at least 50. In addition to the boring data, the data acquired for the current study was used to investigate a ground model using f-k spectra, with the result that the shear velocity near the surface was inferred to be about 140 m/s[18].

Figure 3 shows the arrangement of observation sites in the array. The coordinate axis and observation site names are indicated in the figure. Reference observation site (S0) was taken as the origin for the coordinates. Three-component seismometers were installed at 5 points on each of three lines radiating out from the reference observation site at the center at approximately 120 ° intervals. Hereinafter, the groups of observation sites on the same line will be referred to as Group A, Group B, and Group C as shown in the figure. Also, the observation sites at almost an identical distance (radius) from the reference site will be referred to as Ring 1 to Ring 5 as shown in the figure. The mean diameters of these rings are 2.06 m, 5.29 m, 9.04 m, 14.02 m, and 25.03 m. At observation site A2 (marked in the figure with a white square), the vertical components are clearly abnormal, so the data from this observation site was excluded from the study.

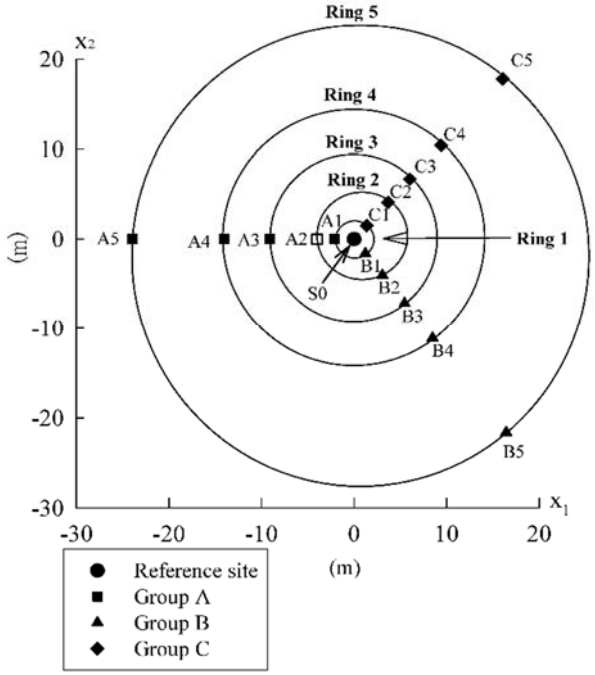

Fig. 3 Small-size dense array configuration

The instruments used for the observations were dual-purpose microtremor detectors and seismometers incorporating servo acceleration sensors as developed by Senna *et al*. (2006)[19]. These instruments were developed for geophysical prospecting, and are frequently used for microtremor observations[20]. We set the sampling intervals to 0.01 s. The observation period was from 15:30 on August 12, 2015 to 01:30 on August 13. Rain fell from 23:30 on August 13, raising the suspicion that microtremor data from that point onwards was affected by rain. There are also roads with heavy traffic near the park. To eliminate the effect of rain and to avoid the effects of traffic as far as possible, analysis was performed on data acquired between 23:00 and 23:30.

3.2 Characteristics of differential acceleration

As stated in Chapter 2, angular acceleration is inferred from differential motion acceleration data (hereinafter, differential motion), which is the difference between the reference site data and the acceleration data a number of other observation sites. Consequently, it is important to investigate the

sort of characteristics that the differential motion has. Figure 4 shows the differential motion for the horizontal x_1 direction component for the observation sites in Group B. The differential motion is based on the observation data for the reference observation site (S0) (see Fig. 3). Before calculating differential motion, the data is passed through a 0.2-8 Hz bandpass filter to eliminate the DC component and the high frequency components. As can be seen from the figure, the greater the distance from the reference site, the greater the differential motion amplitude. This characteristic is similar for the other two components and for the three components of Groups A and C. Next, the characteristics for frequency ranges are investigated.

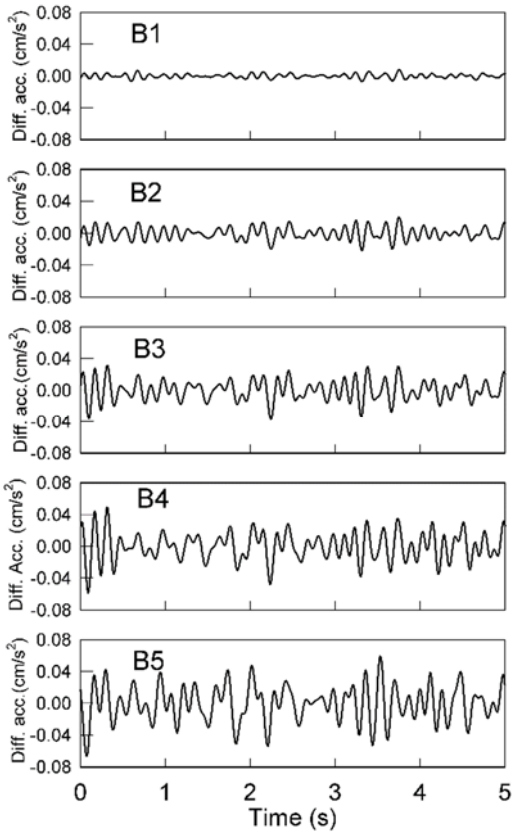

Fig. 4 Example of differential acceleration(x_1 component of Group B), which is the difference between the reference site data and the acceleration data a number of other observation sites

The differential motion power spectra for the horizontal x_1 direction component at each observation site is shown in Fig. 5 for the three groups. Power is large in the 2-8 Hz range, so this range is taken to be the main range covered by this study. As can be surmised from the time-history waveform, for all frequency bands, the spectra increase with distance of the observation site from the reference site. Examining the shapes of the spectra for each observation site, it can be seen that for observation sites closer to the reference site, the spectra increase as frequencies become higher. In contrast, with observations sites further from the reference site, the low frequency components increase. As a result, regardless of the frequency, the shapes of the spectra are either steady or even declining with increasing frequency. The figure depicts only the horizontal x_1 direction components, but the spectra for the horizontal x_2 direction components and vertical x_3 direction components are similar. These spectra characteristics are thought to be due to calculation of differential motion for observation sites close to the reference site canceling the long wavelength (low frequency) components, whereas at distant observation sites, the long frequency components become more difficult to cancel.

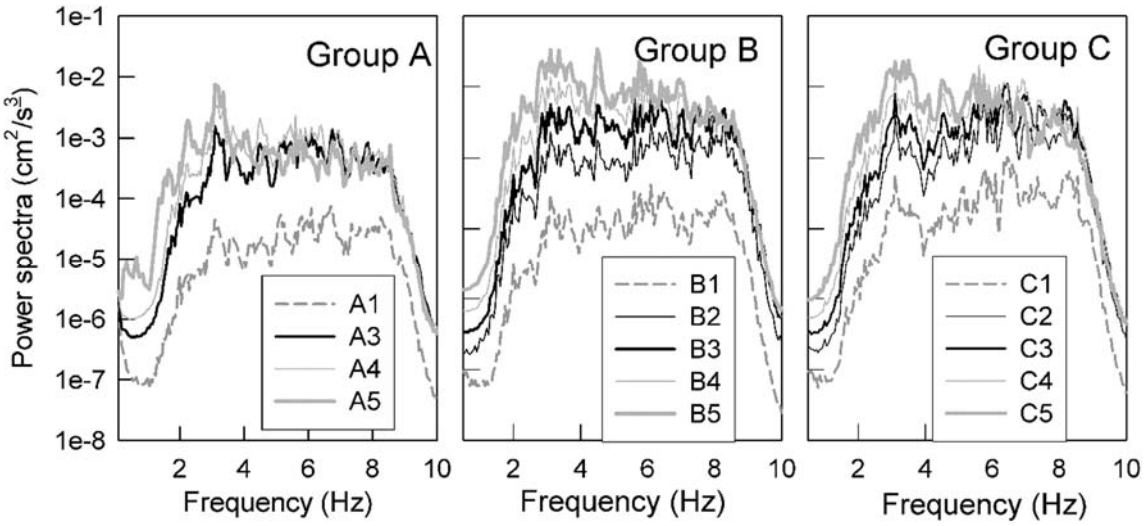

Fig. 5 Differential acceleration x_1 component power spectra

4. ESTIMATION OF ANGULAR ACCELERATION ASSUMING AN ELASTIC BODY

4.1 1st-order elastic method

This section describes inference of rotation components by means of the nth-order elastic method proposed in Section 2. 1. Also, if possible, it describes inference of the zone in which there is behavior as a rigid body with respect to rotation. Before describing these inference processes, it describes the basic approach for inference of rotation components. As can be seen from Eq. (5), $\frac{\partial u_i}{\partial x_1}$ and $\frac{\partial u_i}{\partial x_2}$, the first-order spatial derivatives of acceleration required for inference of rotation components are the gradient of the tangent plane in the x_1 and x_2 directions for the i component differential motion at the reference site. The gradient of the tangent plane can be obtained by two methods. To simplify the explanation here, rather than thinking of two dimensions, it thinks in terms of a certain moment with a single dimension, obtaining the gradient of the tangent to the differential field.

The differential field δu uses the Taylor series expansion with respect to spatial coordinate δx, expressing it as

$$\delta u = a_1 \delta x + a_2 \delta x^2 + a_3 \delta x^3 + \cdots \tag{15}$$

If δx is sufficiently small, the second- and higher-order terms have very little influence, so differential motion field δu can be approximated from the first term alone. In other words, it is possible to obtain the gradient a_1 of the tangent using $\delta u \cong a_1 \delta x$. To obtain the gradient of the tangent by this method, it is necessary for δx to be infinitesimally small, but that is impossible to achieve with actual observations, so differential motion data for an observation site close to the reference site is used. For this reason, there is always doubt as to whether the gradient obtained is an appropriate approximation of the true value. In order to use this approach with data from an array in a two-dimensional plane, only the differential motion for the observation site close to the reference site is applied to the 1st-order elastic method (Eq. (6)) to obtain the rotation components, and as when using a single-dimension array, there is doubt as to whether the inferred rotation components are an appropriate approximation of the true value. Another issue arises when the spatial coordinate δx is large. In such cases, the differential motion field is expressed by a Taylor series expansion including second- and higher order terms, and the coefficient of the first order term with respect to δx is extracted as the gradient. With this method, there is the issue of what order of Taylor series expansion should be used to approximate differential

motion data. When using an array in a two-dimensional plane, the n ($n \geq 2$) th-order elastic method is applied, but it is difficult to determine the appropriate order. As described, there are disadvantages with each method, and consequently it is not possible to demonstrate rigorously that the inferred rotation components are the true rotation components. In this study, the rotation components inferred by both the 1st-order elastic method and the high-order elastic method are assessed together to decide the rotation components.

The approach used for determining the zone within which behavior is taken to be a rigid body with respect to rotation is as follows. With the n ($n \geq 2$) th-order elastic method, since the zone to be taken into account is treated as an elastic body, the inferred angular acceleration is the angular acceleration at the reference site. In contrast, with the 1st-order elastic method, as already stated, since the zone to be taken into account is taken to be a rigid body, the inferred angular acceleration is the angular acceleration of the zone taken into account. Consequently, if the angular acceleration inferred by the nth-order elastic method and the angular acceleration inferred by the 1st-order elastic method are identical, it is possible to take the zone under consideration with the 1st-order elastic method to be a zone that behaves as a rigid body with respect to rotation. Conversely, if the two are not identical, it can be judged that there is no zone behaving as a rigid body.

The remainder of this section describes inference of rotation components by means of a first-order elastic body. The following section describes inference of rotation components by means of an nth-order rigid method, ($n \geq 2$), and based on the approach set out above, obtaining the zone within which angular acceleration behaves as a rigid body.

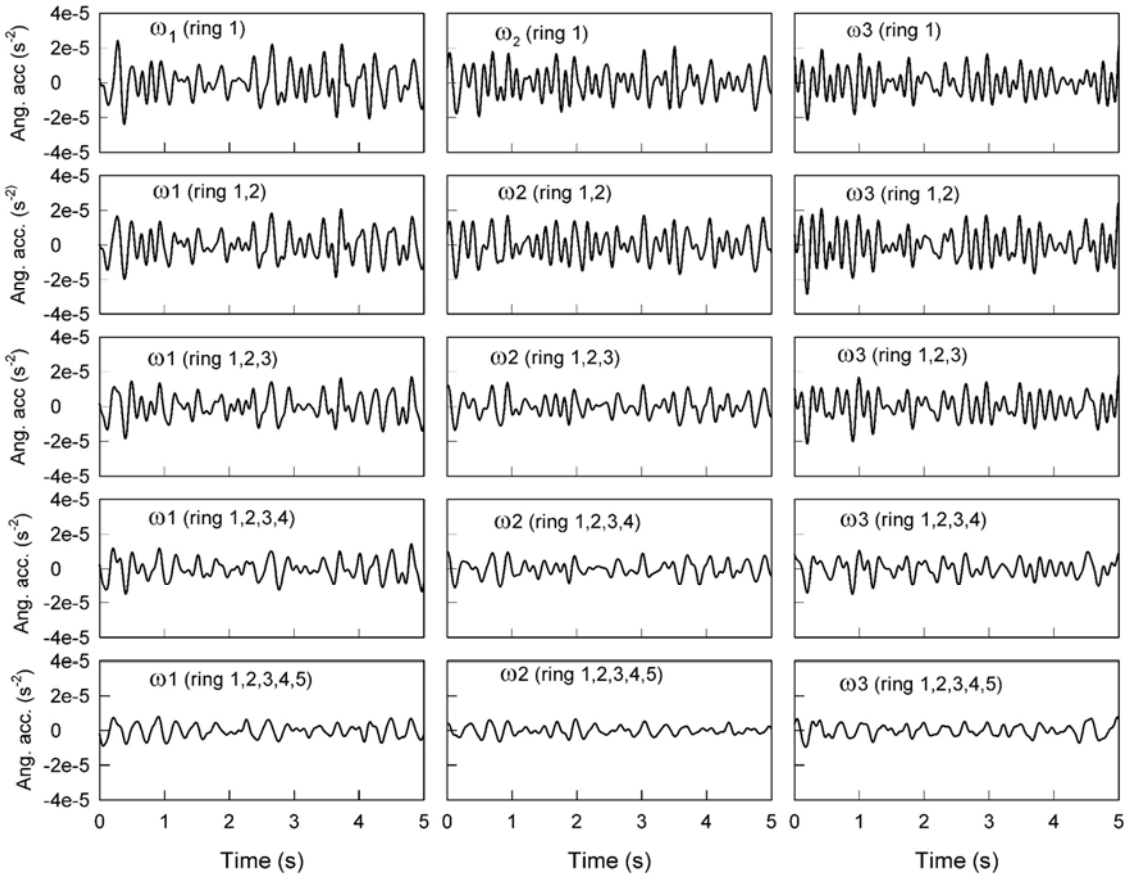

Fig. 6 Results of inference of 3-component angular acceleration $(\omega_1, \omega_2, \omega_3)$, inferred by the 1st-order elastic method

Three-component angular acceleration acquired by the 1st-order elastic method is shown in Fig. 6. If all that needs to be obtained is angular acceleration, it would be sufficient to use a Ring 1 observation

site, which is closest to the reference site, but in order to investigate the zone that behaves as a rigid body with respect to rotation, angular acceleration is also obtained from the differential motion data of observation sites on each of the other rings apart from Ring 1. The three charts in the top row are inferred from the three observation sites of Ring 1. The leftmost shows x_1 angular acceleration (ω_1) with respect to the x_1 axis, the central chart shows angular acceleration (ω_2) with respect to the x_2 axis, and the rightmost shows angular acceleration (ω_3) with respect to the x_3 axis. The second row shows the results of inferring from the differential motion data of the Ring1, 2 observation sites, and the subsequent rows show the subsequent rings (or zones) taken into consideration. The bottom row shows the result of inferring from the differential motion data of the Ring1, 2, 3, 4, 5 observation sites (that is to say, all observation sites). For the Ring 1 3-component rotation waveform and the Ring1, 2 3-component rotation waveform, amplitudes and waveforms resemble each other well, but as the zone taken into account expands to Ring3, Ring4, and Ring 5, the charts show variations, with amplitude decreasing and high-frequency components decreasing, as the difference relative to the angular acceleration waveforms of the top row of charts grows. For the power spectra shown in Fig. 7, as with the results for the time domain, there is a clear decrease in high-frequency components as the zone taken into account expands.

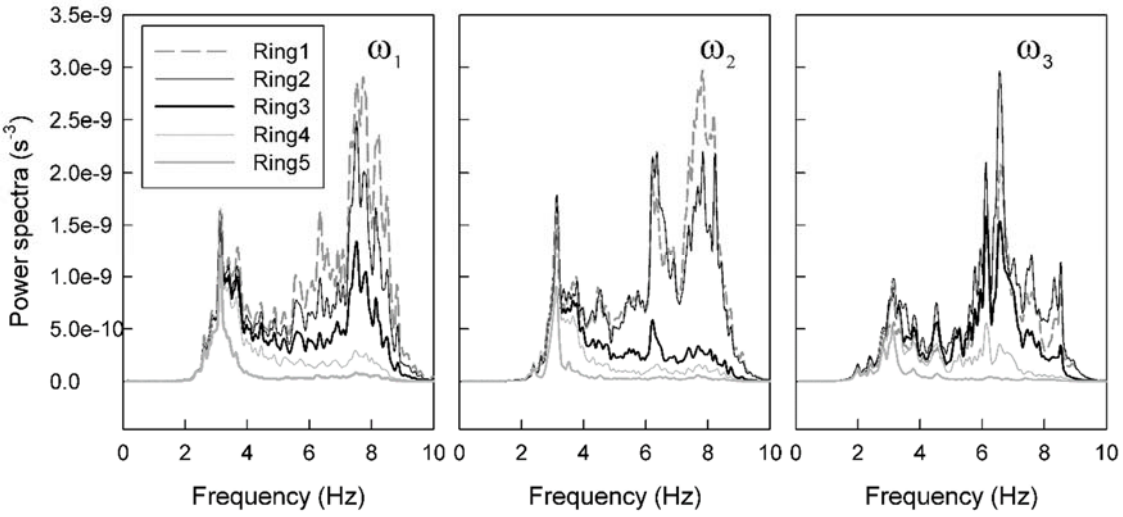

Fig. 7 Power spectra $(\omega_1, \omega_2, \omega_3)$ for the angular acceleration shown in Fig. 6

The accuracy of the rotation components shown in Fig. 6 was inferred. Directly assessing accuracy is not possible because the true rotation components are not clear. Instead, an indirect method is used. Using the observed differential acceleration waveform (abbreviated as "observed differential motion"), and the partial derivatives with respect to spatial variables, the calculated differential acceleration waveforms (abbreviated as "calculated differential motions") obtained from Eq. (6) are compared. In Fig. 8 (a), the results of comparing Ring1 x_1 components shows that both match well. The results for the x_2 components and x_3 components are not shown in the figure, but they also match well. Also for the Ring1, 2 calculated differential motion and observed differential motion shown in Fig. 8 (b), there is a slightly inferior match at observation site A1, but there is a good match for the other four observation sites. Consequently, it is considered that the rotation components can be inferred with very good accuracy from the differential motion of the Ring 1 or Ring1, 2 observation sites. However, when a more expansive zone is used from Ring 3 outwards, the match between the two becomes poor. Figure 8 (c) shows a comparison using all observation sites of Ring1, 2, 3, 4, 5, and the match between the two is very poor. That is to say, it can be seen that if the differential motion taken into account is that for a broader zone from Ring 3 outwards, the rotation components cannot be appropriately inferred with the 1st-order elastic method.

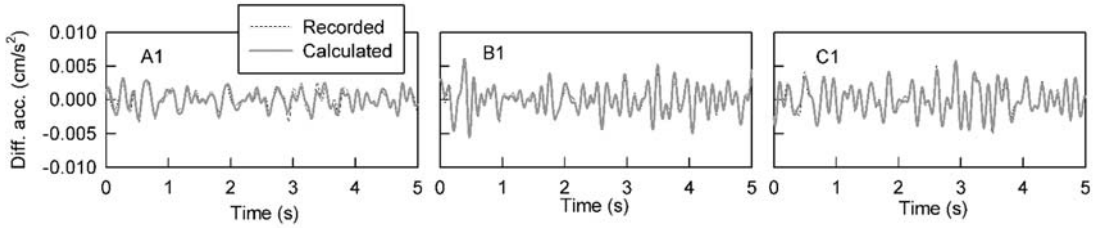

(a) Using differential motion data for ring 1 alone

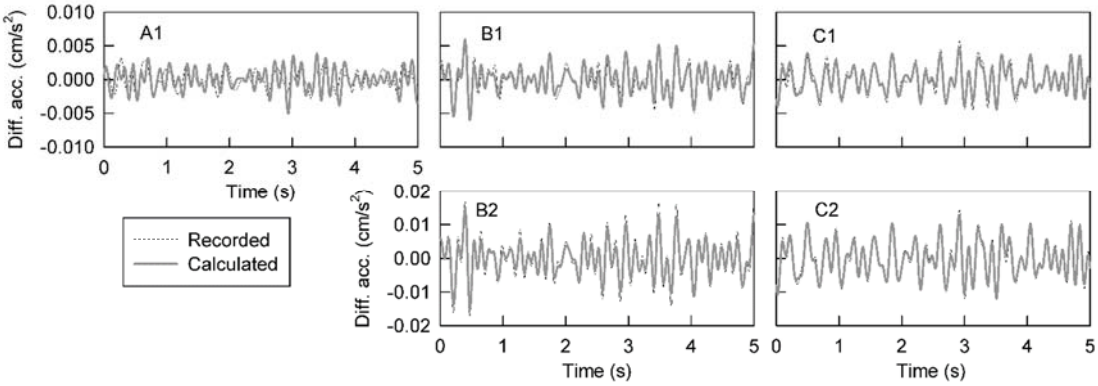

(b) Using differential motion data up to Ring 2

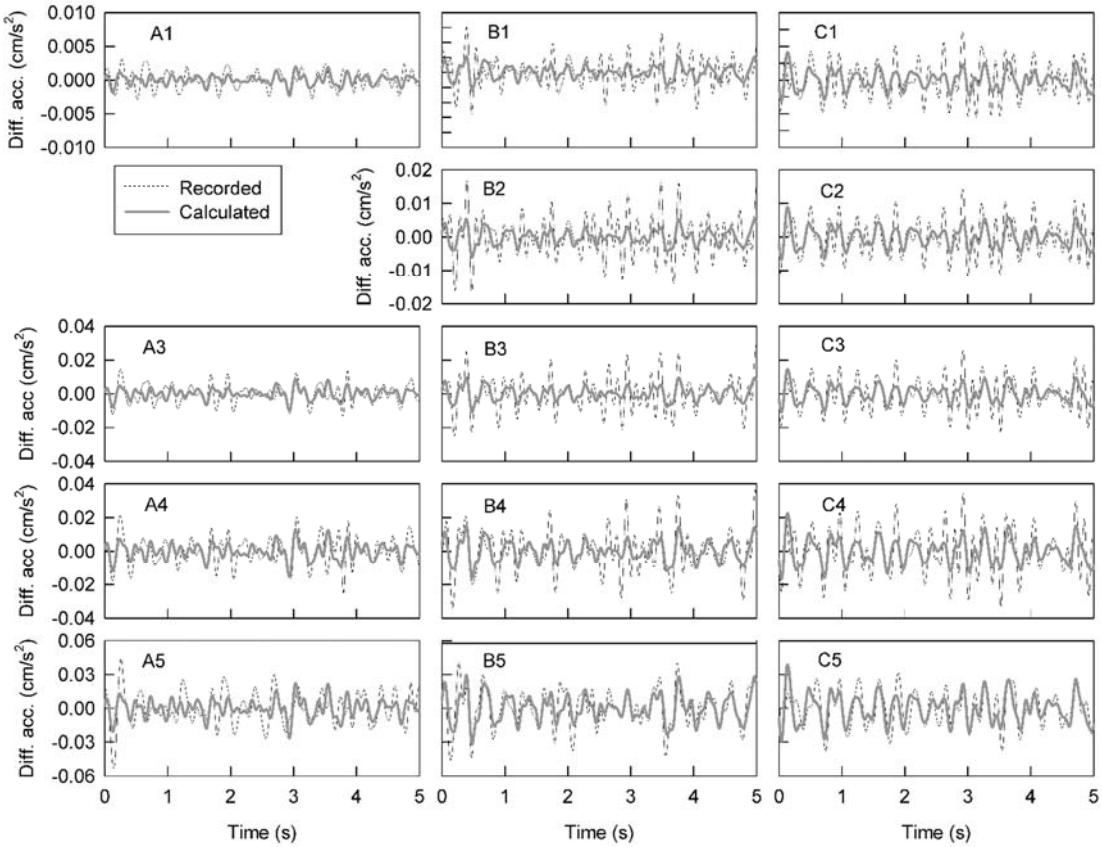

(c) Using differential motion data up to Ring 5

Fig. 8 Comparison of observed differential motion data and differential motion data reproduced using derived functions with the 1st-order elastic method

As already stated above, if the zone taken into account is narrow, a first-order Taylor expansion (that is to say, the 1st-order elastic method) is acceptable, but as the zone taken into account expands, it is necessary to use a higher order Taylor series expansion (that is to say, the nth-order elastic method). For this reason, when obtaining rotation components using differential motion data for a relatively narrow zone such as Ring 1 or Ring 1, 2, it is considered that a reasonable result is obtained from the 1st-order elastic method. However, for wider zones, it is necessary to obtain rotation components using the higher order elastic method. and if the 1st-order elastic method is used, the discrepancy between the observed differential motion and calculated differential motion grows, and as a result, it is considered that a low accuracy inference of rotation components will be achieved.

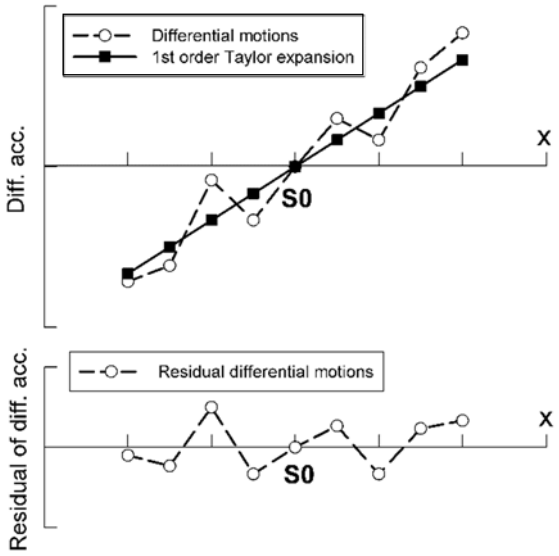

Fig. 9 Schematic showing Taylor series expansion higher-order terms contributing to high frequency angular acceleration

Here, the significance of the Taylor series expansion higher-order terms is examined. To simplify the examination, it is explained in terms of a schematic single-dimension differential motion field at a certain moment (Fig. 9). Using a first-order Taylor expansion to approximate the differential motion field data shown as a dashed line for all observation sites (white circles) is equivalent to approximating the dashed line with the solid straight line seen in the upper panel of the figure. The lower panel shoes the difference between the approximated solid line and the observed values. It can be seen from this figure that there are residuals that cannot be approximated by a straight line. These residuals include a large number of short wavelength (high frequency) components. It can be understood that the 2nd-order and higher terms of the Taylor series expansion are brought in to approximate the high-frequency components included in these residuals. In other words, the approximation of differential motion over a wide zone with a first-order Taylor expansion alone (that is to say, using the 1st-order elastic method) is identical to using spatial smoothing to attenuate the high-frequency components. This way of thinking can be used to understand the characteristics shown in Fig. 7. Taking a wider zone into account means that more high-order terms have to be considered, but in cases where only 1st-order terms are taken into account, the high frequency components are disregarded, so that the amplitudes of inferred rotation components become smaller, and the low frequency components predominate.

From this discussion, it is thought that the zone within which appropriate angular accelerations can be obtained with the 1st-order elastic method is about 5 m from the reference site, to Ring 2 at the most. However, as stated above, although the Ring1, 2 observation sites are relatively close to the reference site, the distance is not infinitesimally small, so there is no guarantee that the Ring 1 or Ring1, 2 rotation components are good approximations of the true rotation components. For this reason, in the next section onwards, the n ($n \geq 2$) th-order elastic method is used to infer rotation components, and results are compared with the rotation components already inferred with the 1st-order elastic method in an attempt

to determine truer components (or good approximations of them). The zone within which there is behavior as a rigid body is also investigated.

4.2 *n* (*n* ≥ 2) th-order elastic method

The rotation components are inferred using the method with the highest order, the 4th-order elastic method. In this case, at least 14 observation sites excluding the reference site are required, so the inference method uses differential motion data for all observation sites in the array shown in Fig. 3. The waveforms inferred for the three rotation components are shown in the second row of Fig. 10. For comparison, the top row shows the angular acceleration waveforms inferred by the 1st-order elastic method from the differential motion data of the 3 observation sites on Ring 1.

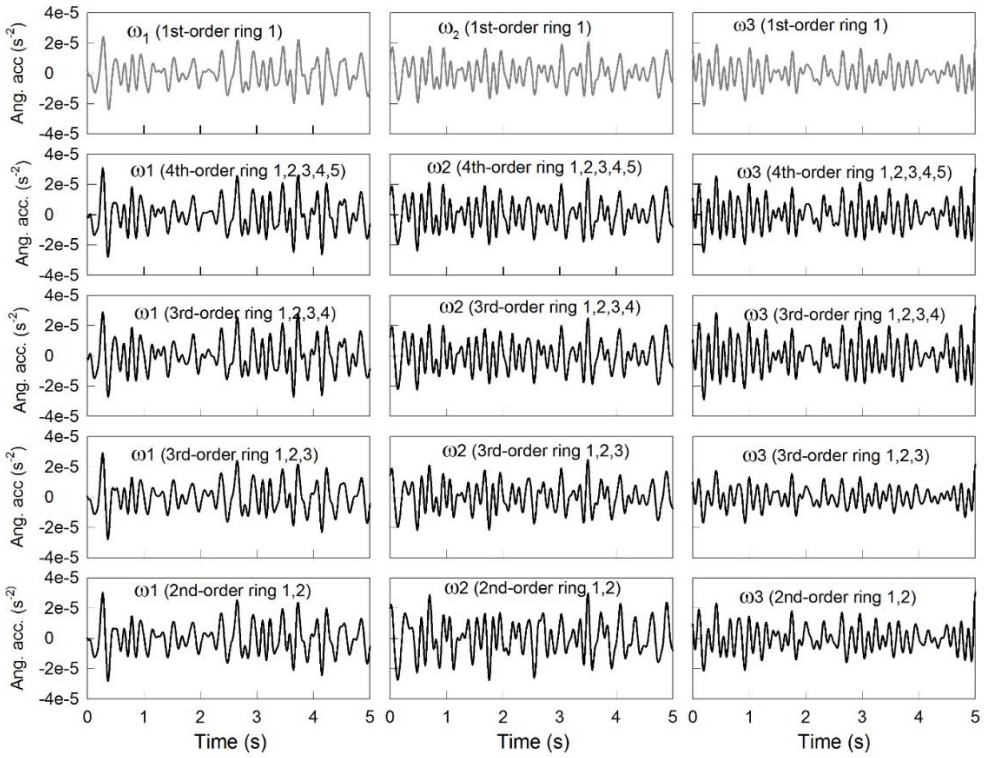

Fig. 10 Results of inference of angular acceleration vector by the highest-order elastic method when using all observation sites on each ring

Before making these comparisons, the accuracy of the rotation components obtained by the 4th-order elastic method was investigated by comparing observed differential motion with calculated differential motion (Fig. 11). As before, only the x_1 components are shown here, but the two motions virtually matched for almost all the observation sites. Compared to the inference by means of the 1st-order elastic method using the differential motion data for all observation sites shown in Fig. 8(c), the match between the observed differential motion and calculated differential motion is improved by a surprising amount. The x_2 components and x_3 components, not visible here, also almost completely matched. This suggests that the rotation components shown in the second row of Fig. 10 are highly accurate. The reason that the observed differential motion and calculated differential motion gave such a good match is thought to be due to taking high-frequency components into account by using the Taylor series expansion up to the 4th order.

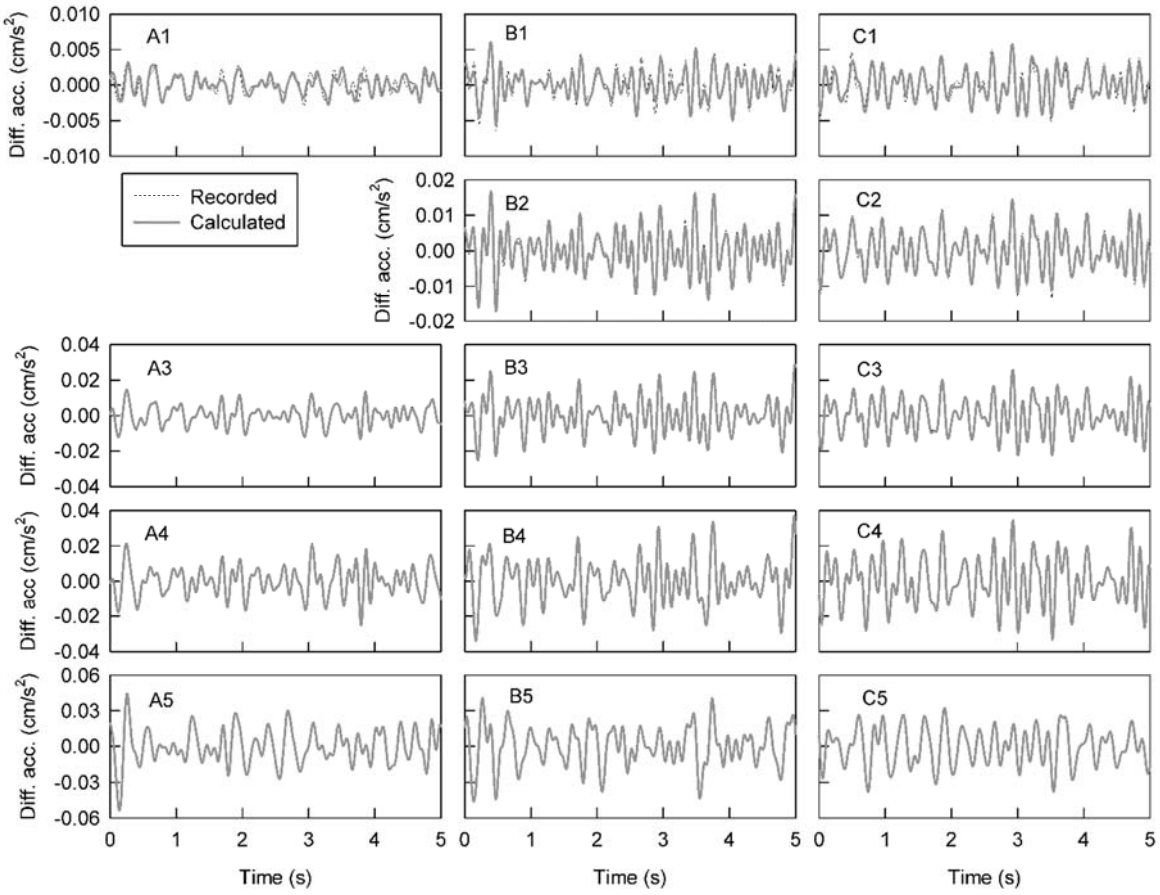

Fig. 11 Comparison of observed differential motion data for all observation sites and differential motion data reproduced using derived functions with the 4th-order elastic method

When the angular acceleration obtained by means of the 1st-order elastic method from differential motion data for the 3 observation sites of Ring 1 shown in the top row of Fig. 10 is compared with the rotation components obtained by the 4th-order elastic method and shown in the second row, the waveforms for the three components resemble each other, but the amplitude of the former is a little smaller than the latter. This suggests that the latter (the rotation components in the 2nd row) is closer to the true rotation components than the former (the rotation components in the 2nd row). This also suggests that the rotation components for Ring 1 or Ring 1, 2 are not the optimum approximation for the true rotation components. To obtain better approximations with the 1st-order elastic method, it is thought that it is necessary to establish new observation sites closer to the reference site than Ring 1.

In the case where the 4th-order elastic method is used, considering three points - the results of comparison between the observed differential motion and calculated differential motion, the results of comparison of the amplitude of rotation components obtained by the 4th-order elastic method and of rotation components obtained by the 1st-order elastic method, and the fact that the 4th-order elastic method contains the highest frequency components - is seems reasonable to judge that the angular acceleration waveforms inferred by the 4th-order elastic method and shown in the 2nd row of Fig. 10 are the best approximation to the true rotation components. In the following discussion, these three angular acceleration waveforms are treated as being an appropriate approximation to the true angular acceleration waveforms.

The discussion up to this point has been based on visual comparison of the rotation components waveforms for a short period of time (5 seconds). Consequently, the reliability of the conclusions is slightly compromised. To address this issue, inferences of rotation components for a longer segment were investigated using the root mean square (RMS) of the inferences to confirm the conclusion

obtained (that the angular acceleration waveforms obtained by the 4th-order elastic method are an appropriate approximation of the true rotation components), and also to investigate the zone behaving as a rigid body with respect to rotation. The RMS amplitude was obtained for the 3-component angular acceleration obtained by means of the 1st-order elastic method for the five different zones of differential motion shown in Fig. 6. The segment used was approximately 10 minutes, a part of the 30-minute record where the influence of local traffic was small (Fig. 12). The RMS amplitude of 3-component angular acceleration obtained by the 4th-order elastic method that is considered to be an appropriate approximation of true angular acceleration was marked as being at the radius zero position. The radius on the horizontal axis represents the mean radius for each ring.

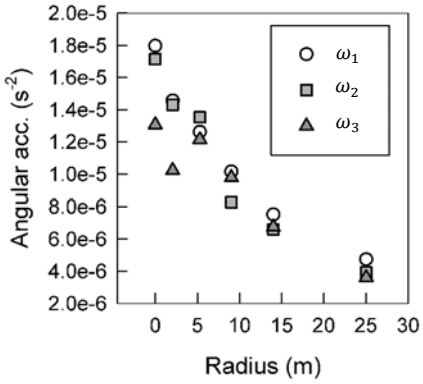

Fig. 12 Comparison of RMS amplitude for the 3 angular acceleration components

The RMS amplitudes of the 2 rocking components shown at the origin were both larger than the RMS amplitude at radius 2.06 m (Ring 1). This result is identical to the result of visual comparison of the rotation components shown on the top row and second row of Fig. 10. That is to say, in the comparison of RMS amplitude, this indicates that the angular acceleration of the 2 rocking components inferred by the 4th-order elastic method is a better approximation of the true angular acceleration than the 3-component angular acceleration obtained from by the 1st-order elastic method from the differential motion data of the 3 observation sites on Ring 1.

Also, the fact that the RMS amplitude is different at the origin and at a radius of 2.06 m indicates that even if there were a limited area where the two rocking components behave as a rigid body, it would be too small to be detectable with the arrangement of the array shown in Fig. 3.

The situation with the torsional component is not the same as with the two rocking components. Its RMS amplitude is greatest at the origin, but it does not differ greatly at radius 2.05 m and radius 2.29 m (Ring2), and appears to be saturated. These three RMS amplitude values for the torsion component show significant scatter, which makes judgment difficult, but suggests the possibility that torsion may be behaving as a rigid body in a zone of about 5 m from the reference site.

The description above has covered the results using differential motion data for all observation sites, but it would also be useful to learn about narrower zones of differential motion data, discovering what sort of relationship there is in such zones between true angular acceleration (in practice, the second row of waveforms in Fig. 10) and angular acceleration inferred using the elastic method with the largest available order. To investigate this issue, the angular acceleration waveforms inferred in the three cases set out below are shown in the third and subsequent rows of Fig. 10.

The third row shows the angular acceleration waveforms, for the three rotation components acquired from differential motion data at the observation sites on Ring 1-Ring 4 by the 3rd-order elastic method.

The fourth and fifth rows show the angular acceleration waveforms for the three rotation components acquired from differential motion data at the observation sites on Ring 1-Ring 3 by the 3rd-order elastic method and on Ring 1-Ring 2 by the 2nd-order elastic method. Observed differential motion and calculated differential motion still matched well in these cases.

What is surprising is that in addition to the 3-component angular acceleration shown in the second row and the 3-component angular acceleration shown in rows 3 to 5 matching well in terms of their

waveforms, they also have well-matching amplitude. This comparison has only been conducted visually, so here too, confirmation is made using RMS amplitude (Fig. 13). The time used for RMS amplitude calculations is the same as used in Fig. 10. For comparison purposes, the RMS amplitude of the 3- component angular acceleration obtained by the 1st-order elastic method from the differential motion data of the 3 observation sites on Ring 1 is also added.

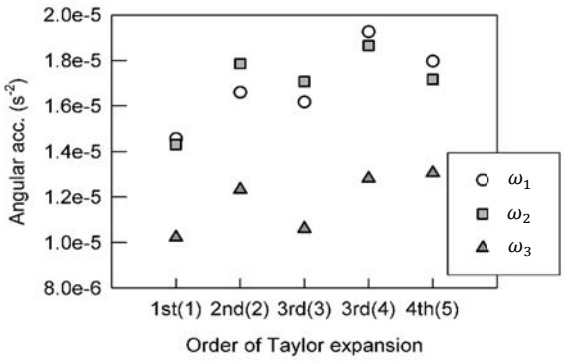

Fig. 13 Estimates of RMS amplitude for the 3 angular acceleration components shown in Fig. 10

The horizontal axis in the figure shows the order of the Taylor series expansion. The figure in parentheses after the figure is the number of the outermost ring used. From Fig. 13, it is possible to confirm statements made above. Specifically, the RMS amplitude of each of the three components of the rotation angle acceleration inferred by the 1st-order elastic method is smaller than the RMS amplitude for any of the remaining four cases.

On the other hand, the RMS amplitude for a particular component is virtually identical to the corresponding component across the four cases. This result is significant because it means that inference of the rotation components is possible with a much simpler array than that shown in Fig. 3. Specifically, it is sufficient to have an array in a narrow zone (extending to about Ring 3) around a reference site, along with enough observation sites (about 10) to be able to use the 2nd- or 3rd-order elastic method. However, this is a conclusion about this particular array, and was obtained in respect of the arrangement of the current array and of the microtremors that were present. Further study would be required before being able to use it unmodified for array observations, particular of seismic waves, because seismic waves differ from microtremors in terms of both group structure (whether surface waves are prominent, or body waves are prominent) and the frequency bands that are of concern. Even obtaining a conclusion with general application to the configuration of arrays for inference of rotation components is outside the scope of this study, and it is difficult to say anything more at this stage. Looking at the details, it has to be said that the RMS amplitude of rotation components obtained by the 3rd-order elastic method from differential motion data for observations sites up to Ring 3 is a little small. The reason is thought to be that with the 3rd-order elastic method, the number of unknown partial derivatives is 9, but the number of observation sites is 8, and as a result, Eq. (5) is underdetermined.

5. ESTIMATION OF ANGULAR ACCELERATION ASSUMING A RIGID BODY

5.1 Multi-site rigid method

If a rigid body is assumed, it is possible to infer rotation components with a small number of observation sites, which has the advantage that observations are simpler. Specifically, at least 3 sites including the reference site are required for the multi-site rigid method, whereas only 2 sites are required for the single-site rigid method. Consequently, in order to be able to make use of this simple observation method assuming a rigid body, it is important to understand the differences and commonalities between assumption of a rigid body and assumption of an elastic body in inference of rotation components.

In section 2.1, it was demonstrated that the 1st-order elastic method and the multi-site rigid method

are identical. The first task here is to confirm that statement. Figure 14 uses differential motion data from observation sites on Ring 1 to compare angular acceleration inferred by the multi-site rigid method and angular acceleration inferred by the 1st-order elastic method. It can be seen that the two match well. Nevertheless, it can also be seen that there are slight differences in the details (particularly for ω_3). The differences are thought to be due to small differences in the inference methods used by these two methods. Specifically, the elastic method uses the weighted least-squares method[14] for inference of differential motion, whereas the multi-site rigid method performs the inference by applying the least-squares method to differential velocity data obtained by numerical integration instead of to differential acceleration data. This is thought to account for the differences. Of course, angular acceleration inferred by the multi-site rigid method displays similar characteristics to angular acceleration inferred by the1st-order elastic method.

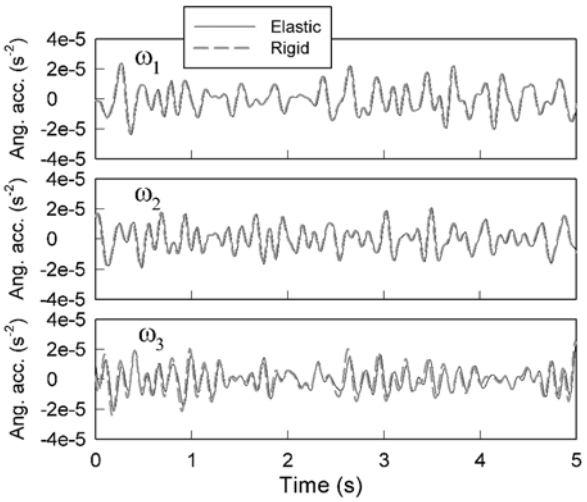

Fig. 14 Comparison of angular acceleration inferred by the multi-site rigid method and the 1st-order elastic method from differential motion data acquired from the observation sites on Ring 1

5.2 Single-site rigid method

The single-site rigid method, which facilitates simpler observations than the multi-site rigid method, is investigated here. Figure 15 shows torsion waveforms inferred by the single-site rigid method for differential motion data for each of the three observation sites on Ring1. The three waveforms are clearly different. From these, it can be understood that it is not appropriate to use torsion waveforms obtained by the single-site rigid method as angular acceleration waveforms. Next, the usability of RMS amplitude is investigated.

First of all, a comparison is made between the RMS amplitude (white and black triangles pointing down) for the two rocking components ω_1 and ω_2 inferred by the 1st-order elastic method and the RMS amplitude for the rocking component ω_r for each observation site in Group A, B, C inferred by the single-site rigid method (Fig. 16). The rocking component ω_r rocks with respect to an axis that passes through the reference site and perpendicular to the axis linking the reference site and observation site. The RMS amplitude of rocking inferred by the single-site rigid method exhibits scattering of inference values between groups but its value increase as the radius becomes smaller. When the RMS amplitudes of the 2 rocking components inferred by the 1st-order elastic method are compared, with the single-site rigid method the RMS amplitude becomes over-large when the radius is large. However, close to the reference site (within a 5 m radius), the values resemble each other well.

A similar comparison is performed for the torsional component (Fig. 17). For Group A, B, C, there is a great deal of scatter in the torsion inferences between the groups, but with the exception of Group A, it exhibits characteristics that are very similar to those of the rocking components. Specifically, when compared to the inference produced by the 1st-order elastic method, with the single-site rigid method

the RMS amplitude becomes over-large when the radius is large. However, close to the reference site (within a 5 m radius), the values resemble each other well.

As noted above, the comparison between 1st-order elastic method and single-site rigid method RMS amplitudes means that close to the reference site, the single-site rigid method RMS amplitude is a guide to RMS amplitude under the 1st-order elastic method. Close to the reference site is the zone where the accuracy of RMS amplitude for rotation components produced by the 1st-order elastic method is high, so this is an important characteristic of RMS amplitude with the single-site rigid method that simplifies observations.

Demonstrating that the single-site rigid method characteristics described above have general application is important for use of its RMS amplitude. As noted in Section 4. 2, with the 1st-order elastic method, the greater the zone taken into account, the stronger the attenuation of high-frequency components due to spatial smoothing. For this reason, inferences are made of angular acceleration, which is only accurate close to the reference site. In contrast, the single-site rigid method only uses the differential motion data for a single observation site, so it cannot perform any smoothing. That is to say, the single-site rigid method does not attenuate any of the high-frequency components, so it takes into account all differential motion frequency components observed. Because of that characteristic, RMS amplitude calculated by the single-site rigid method may be higher than the 1st-order elastic method RMS amplitude when far from the reference site, but is thought to approach the 1st-order elastic method's value when close to the reference site.

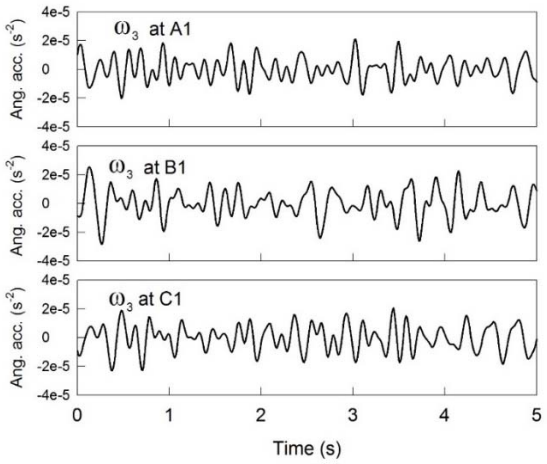

Fig. 15 Comparison of the torsional component inferred by the single-site rigid method for differential motion data at each of the three observation sites on Ring 1

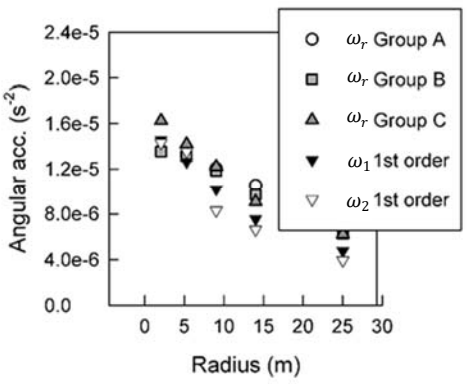

Fig. 16 Comparison of RMS amplitude for rocking inferred by single-site rigid method and 1st-order elastic method

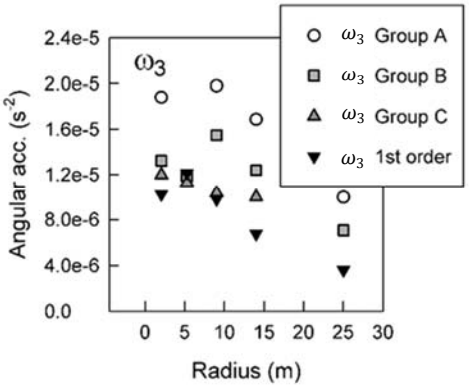

Fig. 17 Comparison of RMS amplitude for torsion inferred by single-site rigid method and 1st-order elastic method

6. SUMMARY AND DISCUSSION

This study describes methods for inference of the rotation components included in seismic motions on a free ground surface using small-size dense array observation data, application of the inference methods to small-size dense array observation data, and findings for finding appropriate rotation components. The results obtained are summarized below.

(1) As methods of inferring angular acceleration using small-size dense array observation data, the study proposes 1) an nth-order elastic method for inferring rotation components from first-order spatial derivatives obtained by the weighted least squares method from differential motions using nth-order Taylor expansions, assuming an elastic body, 2) by the least-squares method and assuming a rigid body, a multi-site rigid method for directly inferring rotation components from multi-point differential motion data, and a single-site rigid method for directly inferring rotation components from single-point differential motion data. In particular, the 1st-order elastic method and multi-site rigid method are identical.

(2) By applying the 1st-order elastic method and 4th-order elastic method to microtremor data acquired by a small-size dense array, the study inferred the angular acceleration of 2 rocking components and a torsional component. It also indicated the possibility that for the torsional component, the ground behaves as a rigid body within a radius of about 5 m.

(3) The study demonstrated that although angular acceleration inferred by the single-site rigid method does not have as much reliability as a waveform, its RMS amplitude can be used as a guide to multi-site rigid method RMS amplitude close to the reference site.

(4) The study found that to obtain the rotation components by an nth-order elastic method, it may be possible to use an array with a simpler configuration than the one used in this research. It also found that, in order to obtain the rotation components by the 1st-order elastic method, it is necessary to establish an observation site closer to the reference site than Ring 1.

The findings of this study were based on data from observation of microtremors with a small-size dense array, but the conclusions above potentially provide a guide for inference of the rotation components of seismic motions by dense array observations.

The authors' study of rotation components was motivated by a question from one of the reviewers when we submitted Hada and Horike[7], a paper in which we demonstrated that Green's functions could be inferred for an 8-story torsionally-coupled shear building with SRC columns and structural steel beams. In that paper we considered the rotation components that we inferred from microtremors on the basement floor to be rotational inputs to the upper floors. The reviewer asked whether the rotation components on the basement floor were due to rotational inputs from the ground. A brief description of the results of our investigation into that question follows.

Ideally, the original survey should have included setting up a small-size dense array near the building and conducting observations at the same time as the microtremor observations in the building. However, for various reasons, including a shortage of usable seismic instruments and issues with finding vacant land near the building, no such small-size dense array observations were made. As an indirect attempt to rectify this omission, we investigated the microtremor data acquired by the small-size dense array in the current study.

If it is assumed that the basement floor is a rigid body, there is no distance from the building's center of gravity for the rotation components. Consequently, the torsional component inferred from the differential motion data of all observation sites within the foundations zone using the 1st-order elastic method (or the multi-site rigid method) can be considered to be the torsional component for the basement floor. The area of the basement floor in the building is about 33×19 m^2. A similar array area would be the zone from Ring 1 to Ring 4 ($\pi \times 13.5^2$ m^2). Using the differential motion data for the 11 observation sites in the Ring 1-Ring 4 zone, we inferred the angular acceleration by the 1st-order elastic method.

Figure 18 shows the angular acceleration inferred. Obtaining the RMS amplitude for torsion (ω_3) gives 5.44×10^{-6} s^{-2}. However, according to the earlier paper, the RMS amplitude for the building's basement floor was 1.76×10^{-6} s^{-2} (See Hada and Horike[7], Fig. 5). These figures mean that if the

building had been constructed in the park where we used the small-size array, the torsion RMS amplitude would be approximately three times the figure for the location where the building is actually constructed. Similarly, the horizontal component microtremor RMS amplitude in the park was found to be approximately three times the horizontal component microtremor RMS amplitude measured on the ground surface close to the building. Taking into account differences in microtremor levels between the building's location and the park, this means that it is acceptable to consider the torsion in the building's basement floor to be rotational inputs. This discussion lacks rigor, but the rotation components inferred from the microtremors in the basement floor can be considered to provide indirect evidence of being due to rotation components in the ground.

There are plans to publish the software created for the purposes of this study (nth-order elastic method and nth-order rigid method). Potential users are invited to contact the authors.

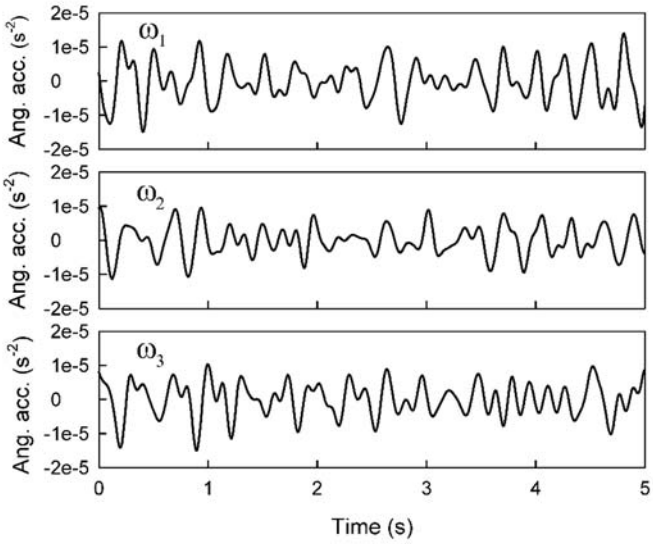

Fig. 18 Three-component angular acceleration inferred by the 1st-order elastic method using differential motion data from observation sites in the building's basement zone

ACKNOWLEDGMENT

The authors would like to thank the students in the Horike Lab at Osaka Institute of Technology in 2015 for their assistance in acquiring the microtremor observation results used in this paper. We also thank the three anonymous reviewers for their comments and for helping to improve the paper.

REFERENCES

1) Osawa, Y., Murakami, M. and Kitagawa, Y.: A Brief Report on the Damage to Buildings during the 1968 Off Tokachi Earthquake. *Bulletin of the Earthquake Research Institute, University of Tokyo*, Vol. 46(6B), pp. 1451–1459, 1968. (in Japanese)
2) Architectural Institute of Japan: *1968-nen Tokachi Oki Chishin Saigai Chosahokokusho ("1968 Off Tokachi Earthquake Survey Report")*, Architectural Institute of Japan, 1968. (in Japanese)
3) Architectural Institute of Japan: *1978-nen Miyagi Ken Oki Jishin Saigai Chosahokokusho ("1978 Off-Miyagi Earthquake Survey Report")*, Architectural Institute of Japan, 1980. (in Japanese)
4) Architectural Institute of Japan: *Preliminary reconnaissance report of the 1995 Hyogoken-Nanbu earthquake*, Architectural Institute of Japan, 50 p. and 142 p., 1995. (in Japanese)
5) Architectural Institute of Japan: *2016-nen Kumamoto Jishin Saigai Chosahokokukai ("2016 Kumamoto Earthquake Survey Report Meeting")*, Architectural Institute of Japan Research

Committee on Earthquake Disaster, pp. 2–4 and pp. 39–46, 2016. (in Japanese)
6) Shibata, A.: *Saishin Taishin Kozo Kaiseki 2 ("Latest Aseismic Structure Analysis 2")*, Morikita Publishing, pp. 265–272, 2003. (in Japanese)
7) Hada, K. and Horike, M.: Inference of Green's Functions for Torsionally Coupled Buildings from Microtremor Recordings and Their Reliability as well as Their Characteristics, *Journal of Structural and Construction Engineering*, Architectural Institute of Japan, Vol. 80, No. 714, pp. 1239–1249, 2015. (in Japanese)
8) Yagi, S., Fukawa, N. and Tobita, J.: Influence of Rotational Foundation Input Motion Due to Rayleigh Wave on Transfer Function Estimation of Low-rise R.C. Buildings Based on Microtremor Observation, *Journal of Structural and Construction Engineering*, Architectural Institute of Japan, No. 552, pp. 77–84, 2002. (in Japanese)
9) Ghayamghamian, M. R. and Nouri, G. R.: On the Characteristic of Ground Motion Rotation Components Using Chiba Dense Array Data, *Earthquake Engineering and Structure Dynamics*, Vol. 36, pp. 1407–1429, 2007.
10) Basu, D., Whittaker, A. S. and Constantinou, M. C.: Extracting Rotational Components of Earthquake Ground Motion Using Data Recorded at Multiple Stations, *Earthquake Engineering and Structure Dynamics*, Vol. 42, pp. 451–468, 2016.
11) William, H. K. Lee., Bor-Shouh, Huang., Charles, A. Langston., Chin-Jen, Lin., Chun-Chi, Liu., Tzay-Chyn, Shin., Ta-Liang, Teng. and Chien-Fu, Wu.: Review: Progress in Rotational Ground-Motion Observation from Exploration and Local Earthquakes I Taiwan, *Bulletin of the Seismological Society of America*, Vol. 99, No. 2B, pp. 958–967, 2009.
12) Katayama, T., Yamazaki, F., Nagata, S. and Sato, N.: Earthquake observation by a three-dimensional seismometer array and its strong motion database, *Proceedings of the Japan Society of Civil Engineers*, No. 422/I–14, pp. 361–369, 1990. (in Japanese)
13) Aki, K. and Richards, P. G.: *Quantitative Seismology, Second Edition*, University Science Books, Sausalito California, pp. 12–13, 2002.
14) Menke, W.: *Geophysical Data Analysis: Discrete Inverse Theory Revised Edition*, Academic Press Inc., pp. 45–46, 2002.
15) Spudich, P., Steck, L. K., Hellweg, M., Flecher, J. B. and Baker, L.: Transient Stress at Parkfield, California, Produced by the M 7. 4 Landers Earthquake of June 28, 1992: Observation from the UPSAR Dense Seismograph Array, *Journal of Geophysical Research*, Vol. 100, pp. 675–690, 1995.
16) Sogo, K., Wadachi, M. and Deguchi, T.: *Mechanics from zero II*, Iwanami, pp. 98–99, 2005. (in Japanese)
17) Ministry of Land, Infrastructure, Transport and Tourism: KuniJiban (search site for national geotechnical information), http://www.kunijiban.pwri.go.jp. (in Japanese, last accessed on March, 2017)
18) Tsuchida, K., Horike, M., Ito, S. and Hada, K.: Comparison of two horizontal phase velocities by the f k spectrum estimated using two different maximum likelihood methods, *Programme and Abstracts, the Seismological Society of Japan, Fall Meeting*, S16–P07, 2016. (in Japanese)
19) Senna, S., Adachi, S., Ando, H., Araki, T., Iisawa, K. and Fujiwara, H.: Development of microtremor survey observation system, *Proceeding of the Society of Exploration Geophysicists of Japan Conference 115*, pp. 227–229, 2006. (in Japanese)
20) Goto, H., Hada, K., Sawada, S., Yoshida, N. and Ouchi, T.: Evaluation of site response on downtown area of Namie town, Fukushima, based on microtremor and aftershock observation. *Journal of Japan Association for Earthquake Engineering*, Vol. 16, No. 1, pp. 309–321, 2016. (in Japanese)

(Original Japanese Paper Published: May, 2017)
(English Version Submitted: June 2, 2019)
(English Version Accepted: July 14, 2019)